Journal of Science: Advanced Materials and Devices 6 (2021) 595–600

Contents lists available at ScienceDirect

Journal of Science: Advanced Materials and Devices

journal homepage: www.elsevier.com/locate/jsamd

Original Article

The atomic and electronic structure of $Hf_{0.5}Zr_{0.5}O_2$ and $Hf_{0.5}Zr_{0.5}O_2$:La films

Timofey V. Perevalov [a, b], Igor P. Prosvirin [c, *], Evgenii A. Suprun [c], Furqan Mehmood [e], Thomas Mikolajick [d, e], Uwe Schroeder [e], Vladimir A. Gritsenko [a, b]

[a] Rzhanov Institute of Semiconductor Physics SB RAS, 13 Lavrentiev Ave., 630090, Novosibirsk, Russia
[b] Novosibirsk State University, 2 Pirogov Str., 630090 Novosibirsk, Russia
[c] Boreskov Institute of Catalysis, SB RAS, 5 Lavrentiev Ave., 630090, Novosibirsk, Russia
[d] NaMLab gGmbH, Noethnitzer Str. 64 a, 01187 Dresden, Germany
[e] Chair of Nanoelectronics, TU Dresden, 01062 Dresden, Germany

ARTICLE INFO

Article history:
Received 19 April 2021
Received in revised form
24 June 2021
Accepted 3 August 2021
Available online 11 August 2021

Keywords:
FeRAM
XPS
Oxygen vacancy
Electronic structure
HfZrO

ABSTRACT

$Hf_xZr_{1-x}O_2$ and lanthanum-doped $Hf_xZr_{1-x}O_2$:La thin films are candidates for applications in ferroelectric random-access memory. Here, we explore the atomic and electronic structure of $Hf_{0.5}Zr_{0.5}O_2$ and $Hf_{0.5}Zr_{0.5}O_2$:La thin films grown by atomic layer deposition. Using X-ray photoelectron spectroscopy, it was found that the oxides under study have an almost identical electronic structure and a bandgap of about 5.4 eV. The $Hf_{0.5}Zr_{0.5}O_2$:La film was shown to consist of the mixture of $Hf_{0.5}Zr_{0.5}O_2$ and La_2O_3 phases. The bombardment with argon ions of the studied films leads to oxygen vacancy generation in the near-surface layer. The oxygen vacancy concentrations in the bombarded films were evaluated from the comparison of experimental valence band photoelectron spectra with the theoretical ones calculated using the density functional theory.

1. Introduction

Currently, $Hf_xZr_{1-x}O_2$ thin films are considered to realize ferroelectric random-access memory (FeRAM) as the most promising candidates for scalable nonvolatile memory [1]. It was found that the thin $Hf_xZr_{1-x}O_2$ films doping with lanthanum significantly improves the endurance, i.e. number of read/write cycles, of FeRAM capacitors [2,3]. The ferroelectric properties of hafnia based materials are usually explained by the noncentrosymmetric (polar) orthorhombic phase (*Pca*21) stabilization that allows the spontaneous polarization of the oxide (ferroelectric effect) [4–6]. Ferroelectric $Hf_xZr_{1-x}O_2$ and $Hf_xZr_{1-x}O_2$:La thin films are compatible with silicon technology and could replace perovskite films in the traditional FeRAM [1].

The ferroelectric capacitor endurance is correlated with the leakage current and, thus, with the charge transport and defect generation. It is well known that the electronic and transport properties of hafnia and zirconia-based dielectrics, as well as $Hf_xZr_{1-x}O_2$, are mainly determined by oxygen vacancies [7–11]. Oxygen vacancies in $Hf_xZr_{1-x}O_2$ act as traps for charge carriers and are formed during the dielectric degradation of the ferroelectric capacitor [10,12]. The oxygen vacancies in the dielectric layer affect the ferroelectric properties, such as polar orthorhombic phase stabilization [13], polarization switching voltage, number of switched domains and breakdown voltage [6,14]. To improve the properties of ferroelectric layers, it is necessary to know the atomic and electronic structure of oxygen vacancies in $Hf_xZr_{1-x}O_2$ and $Hf_xZr_{1-x}O_2$:La. Currently, a lot of investigations are devoted to HfZrO-based ferroelectric capacitors [15,16], but the atomic and electronic structure of $Hf_xZr_{1-x}O_2$:La and $Hf_xZr_{1-x}O_2$:La having oxygen deficiencies remain unclear.

The standard method for hafnia-based ferroelectric thin film synthesis is that of atomic layer deposition (ALD). Such films are nearly stoichiometric, so that for high-k oxide dielectrics the native defects (oxygen vacancies) concentration is typically below 10^{18} - 10^{19} cm^{-3} [8,10]. Such low defect concentration is still enough to determine the charge transport. However, such a concentration level is too low to study the atomic and electronic structure of

* Corresponding author.
E-mail address: prosvirin@catalysis.ru (I.P. Prosvirin).
Peer review under responsibility of Vietnam National University, Hanoi.

https://doi.org/10.1016/j.jsamd.2021.08.001

oxygen vacancies using photoelectron spectroscopy. To increase the oxygen vacancy concentration, one can use the phenomenon of partial metal reduction by the Ar^+- ion bombardment. Such an approach was previously used for the oxygen vacancy generation in HfO_2 [17], HfO_2:La [18] and HfZrO [19] films. Another method to determine the electronic structure of oxygen vacancies is quantum-chemical calculations using the density functional theory (DFT).

This work aims at characterizing and comparing the atomic and electronic structure of $Hf_{0/5}Zr_{0.5}O_2$ and $Hf_{0.5}Zr_{0.5}O_2$:La with low and high oxygen vacancy concentrations.

2. Experimental

Ferroelectric $Hf_{0.5}Zr_{0.5}O_2$ (HZO) and La-doped $Hf_{0.5}Zr_{0.5}O_2$ (HZLO) films with a thickness of about 25 nm were synthesized by the ALD on a silicon substrate. $Hf[NC_2H_5CH_3]_4$ (TEMAH), $Zr[NC_2H_5CH_3]_4$ (TEMAZ) in equal mass concentrations, and $La(iPrCp)_3$ (tris(isopropyl-cyclopentadienyl)lanthanum) were used in the Oxford Instruments OPAL system as hafnium, zirconium, and lanthanum precursors, respectively. Oxygen plasma was used as an oxidant for La, while H_2O was utilized for Hf and Zr ALD cycles. The samples were then annealed at 500 °C for 1 min in the N_2 atmosphere. A La content of about 3.5% was calculated from the corresponding growth rate values and cycle ratios. Since only a small amount of the La_2O_3 interlayer is introduced in the $Hf_{0.5}Zr_{0.5}O_2$ layer and the La atoms are not uniformly distributed, a structural characterization method would not be able to determine a more precise La content.

The morphological and structural analysis of the thin film surfaces before and after Ar^+ bombardment was made using Tescan Solaris S900 FIB/SEM system. Micrographs of the surface and cross-section of the film were obtained in the SE (secondary electrons) mode at electron beam energy of 20 keV and a current of 1 nA. The parameters of measurements by the FIB (Ga^+ ions) method were as follows: ion beam energy of 30 keV and a current of 250 nA. The cross-section size was 2 × 0.2 μm.

The X-ray photoelectron spectra (XPS) were measured using a SPECS spectrometer with a PHOIBOS-150-MCD-9 analyzer and a FOCUS-500 monochromator (Al K_α radiation, hν = 1486.74 eV, 200 W). The peaks binding energy (BE) was calibrated by the C1*s* peak position (284.8 eV), corresponding to the surface hydrocarbon-like deposits. The survey spectrum and the narrow spectra (valence band, Hf4*f*, Zr3*d*, C1*s*, O1*s* and La3*d*) were registered at the analyzer pass energy of 20 eV. The atomic ratios of the elements were calculated from the integral photoelectron peak intensities, which were corrected by the corresponding sensitivity factors based on Scofield photoionization cross-sections. The Shirley method was used for the background subtraction. A convolution of Gaussian and Lorentzian functions was used for fitting the Hf4*f*, Zr3*d* and O1*s* peaks. The ion bombardment of the sample was performed using an ion gun (SPECS, model IQE 11/35) for the oxygen vacancy generation. The Ar^+ ion energy, current density, treatment time and beam angle were 1.25 keV, 8–10 μA/cm^2, 5 min, and 45°, respectively.

The valence band XPS was calculated from the first principles with the density functional theory using the Quantum ESPRESSO software package [20]. The defect-free crystals and crystals with a single oxygen vacancy in $Hf_{0.5}Zr_{0.5}O_2$ and $Hf_{0.5}Zr_{0.5}O_2$:La in the orthorhombic non-centrosymmetric phase *Pca*2$_1$ (o-HZO and o-HZLO) were modelled. o-HZLO is obtained by replacing two adjacent metal atoms with La in a 96-atom supercell, which corresponds to a doping level of ≈2.1 at.%, and removing one common 3-coordinated oxygen atom. The hybrid functional B3LYP was used, and it gives the o-HZO bandgap value 5.6 eV. The XPS spectrum was calculated by summing the spectra of the projected density of electronic states smoothed by the Gaussian function with σ = 0.5 eV. The weight coefficients were obtained from the best agreement of the calculation for defect-free HZO and the experimental value fo the pristine HZO film.

3. Results and discussion

Analysis of scanning electron microscopy (SEM) images of the HZLO sample revealed that the initial film exhibits a granular polycrystalline structure, with a granule (domain) size of about 10–50 nm (Fig. 1a). This is the expected result [21] (Fig. 1a). The surface morphology of the film does not change after the Ar^+ ion bombardment (Fig. 1b). Therefore, the bombardment mode used does not lead to etching film. However, after argon treatment, the film became more heterogeneous, as evidenced by the blurred SEM images. The film thickness before and after Ar^+ ion bombardment remains unchanged and is about 25 nm (Fig. 1c,d).

The Hf4*f* and Zr3*d* XPS of the initial HZO and HZLO samples can be well approximated by single doublets (Fig. 2). The position of the Hf4$f_{7/2}$ maximum at the energy of 17.0 eV corresponds to the Hf^{4+} state and coincides with the energy position of the same maximum in HfO_2 [22,23]. The difference in the binding energy values of the O1*s* and Hf4*f* levels for the studied samples is 513.2 eV and it coincides with the corresponding HfO_2 value. Similarly, the maximum of Zr3$d_{5/2}$ at 182.3 eV corresponds to the Zr^{4+} state and coincides with the reported data for stoichiometric ZrO_2 [24,25]. It seems that Hf and Zr are mainly present in the measured samples as HfO_2 or ZrO_2, respectively. However, we cannot conclude unequivocally that the samples consist of a HfO_2 and ZrO_2 mixture since these oxides have almost identical atomic and electronic structures.

A bombardment of the samples with Ar^+ ions leads to the broadening of the Hf4*f* and Zr3*d* peaks towards lower binding energies. This indicates a partial disorder of the near-surface region and the defects formation under the influence of the ion beam. For the HZO sample, the full width at a half height (FWHM) for the Hf4*f* peak increases from 1.12 eV to 1.15 eV, and for the Zr3*d* – from 1.18 eV to 1.23 eV. For the HZLO sample, the corresponding FWHM values are 0.03 eV less, compared to the HZO films. The deconvolution of Hf4*f* and Zr3*d* lines into separate components revealed additional peaks with the energy values at 16.2 eV and 181.3 eV, respectively. These peaks are characteristic for Hf and Zr in relevant nonstoichiometric oxides (HfO_{2-x} and ZrO_{2-x}), where the metal atoms have low oxidation states (1+, 2+, 3+) [26,27]. The presence of Hf and Zr states with the oxidation degree lower than in HfO_2 and ZrO_2 is naturally explained by the generation of a high concentration of oxygen vacancies in the films under the influence of the Ar^+ ion beam.

The O1*s* XPS deconvolution to individual components shows two peaks with the maxima at the energies of 530.2 eV and 531.8 eV, respectively (Fig. 2c). The first peak can unambiguously be attributed to the lattice oxygen in HfO_2 and ZrO_2. The second one is characteristic for weakly bound adsorbed oxygen on the sample surface. After the Ar^+ ion treatment the oxygen content adsorbed on the surface was significantly reduced.

The O1*s* XPS reflects the photoelectron energy loss spectrum on the electron excitation from the valence band to the conduction band, which allows estimating the bandgap value E_g. It is determined by the linear interpolation of that spectrum edge to the background level (Fig. 3). For samples HZO and HZLO, the

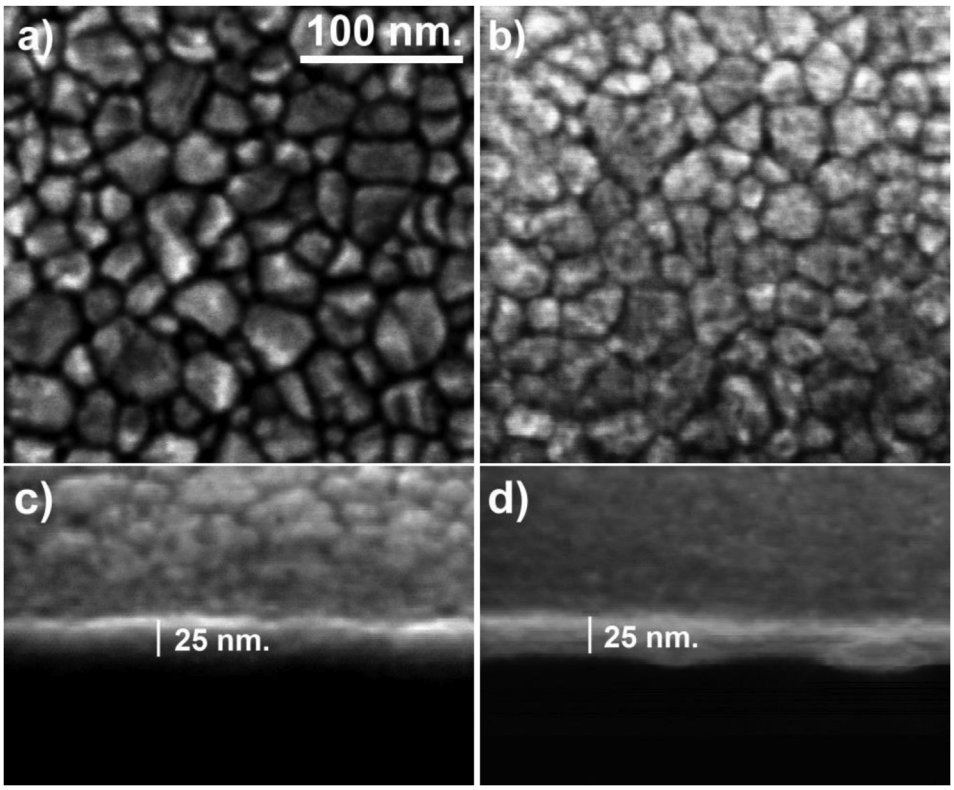

Fig. 1. SEM micrographs of HZLO sample before (a,c) and after (b,d) Ar^+ bombardment.

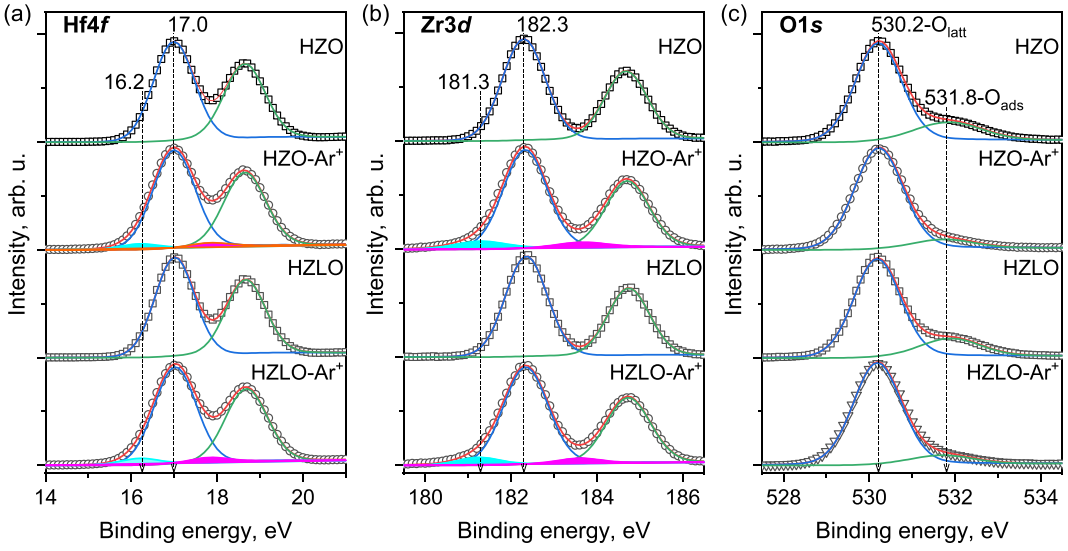

Fig. 2. Hf4*f* (a), Zr3*d* (b) and O1*s* (c) XPS of HZO and HZLO samples before and after Ar^+ bombardment.

energy loss spectra of O1*s* photoelectrons are almost identical and the E_g value was estimated as 5.4 ± 0.1 eV. This result is consistent with the E_g value at 5.37 eV calculated earlier for $Hf_{0.5}Zr_{0.5}O_2$ from the transmission spectra [28] and the value of 5.3 eV obtained from the photoelectron spectra [29]. Thus, the HfZrO doping with La to a concentration of up to 3.5 at.% does not change the bandgap.

The La3$d_{5/2}$ XPS for the HZLO sample consists of the main peak at 834.1 eV and a satellite at 836.8 eV, which is typical of La^{3+} state in La_2O_3 [30–32] (Fig. 4). The satellite is attributed to the process in which the electron density shifts from filled O2*p* to empty La^{3+} 4*f* levels (the so-called shake-up satellite) [33]. The difference between the binding energy values for the La^{3+} satellite and the main peak of La3$d_{5/2}$ is 4.7 eV. This value is typical of La_2O_3, whereas, for lanthanum hydroxide, this value lies in the range of 3.6–3.9 eV [31,34]. Thus, the XPS of La3$d_{5/2}$ indicates that the La atoms in HZLO are mainly included in La_2O_3. The La3$d_{5/2}$ main peak FWHM for the initial sample is 2.05 eV and it increases to 2.2 eV after the Ar^+ bombardment. That indicates the partial disordering of the film surface region (structural defects formation).

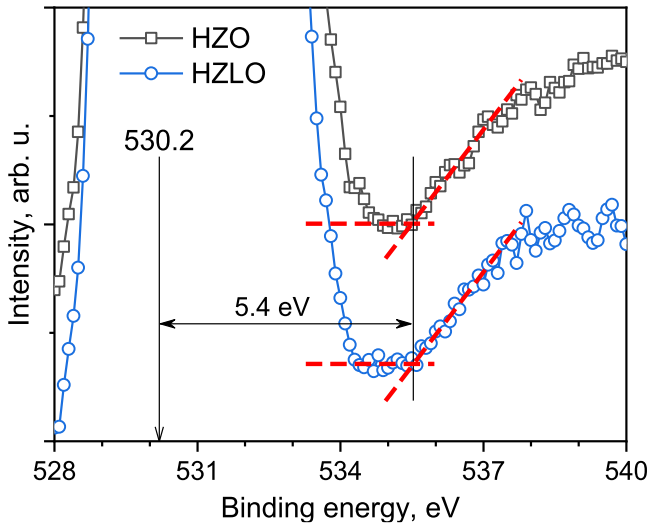

Fig. 3. Fragment of the XPS O1*s* of HZO and HZLO initial samples, illustrating the method for bandgap value determining.

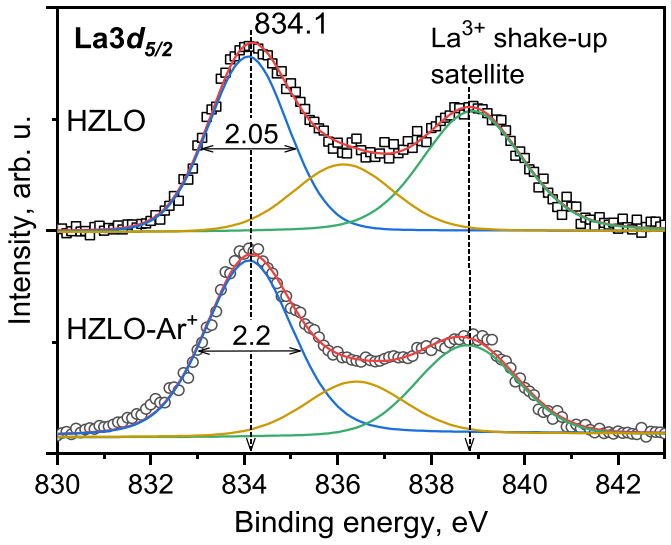

Fig. 4. La3$d_{5/2}$ XPS of HZLO sample before and after Ar^+ bombardment.

Table 1
The near-surface layer (at.%) composition of HZO and HZLO samples before and after Ar^+ ions bombardment.

Samples	Hf	Zr	O	C	La
HZO	12.0	14.8	47.3	25.9	–
HZO-Ar^+	16.4	18.1	59.0	6.6	–
HZLO	11.7	14.3	45.9	27.6	0.9
HZLO-Ar^+	16.2	17.6	58.4	7.2	1.0

The elements atomic ratios for the HZO and HZLO samples before and after the Ar^+ ion bombardment are shown in Table 1. The atomic ratio [Zr]/[Hf]~1.2 differs from that expected for HZO and HZLO films (~1) that can be explained by a different degree of screening of Hf and Zr by adsorbates, by different free path lengths λ of Hf4*f* and Zr4*f* photoelectrons and by the inaccuracy of the atomic sensitivity coefficient values. After the Ar^+ ion treatment, the carbon concentration on the surface decreases significantly, and the films composition changes slightly. The [O]/[Zr+Hf] atomic ratio 1.76 and 1.77 for the initial HZO and HZLO films are decreases to a value of about 1.71 and 1.73, respectively after the Ar^+ ion bombardment. Taking into account the normalization for the initial HZO film to the stoichiometric oxide [O]/[Hz+Zr] = 2, the argon bombardment reduce the atomic ratio to 1.94 and 1.96 for HZO and HZLO films respectively. The obtained La low content value of about 1 at.% in the HZLO film can be explained by its nonuniform distribution. Similar values were reported by Hamouda et al. before [16].

The valence band photoelectron spectrum shows that, after the Ar^+ bombardment, a low-intensity peak appears above the valence band edge (Fig. 5). The experimental spectra are well described by the peaks calculated from the first principles for ideal o-HZO and o-HZLO crystals and crystals with oxygen vacancies. The agreement between the calculation and the experiment indicates the correctness of the used theoretical model. The calculated spectra of the crystals with oxygen vacancies show a peak in the bandgap

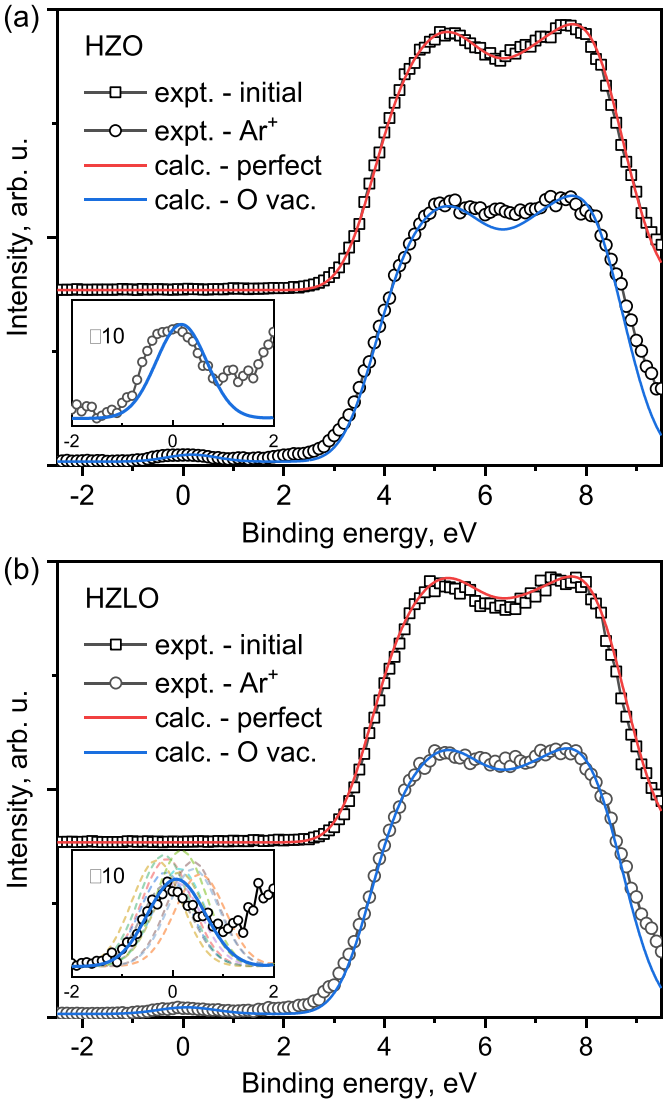

Fig. 5. Valence band XPS of the HZO (a) and HZLO (b) samples before and after ion bombardment (symbols), as well as the calculated ones for the perfect crystals and for crystal with differently coordinated O vacancies (lines). On the figure (b) the dashed lines in the inset are the calculated spectra for 12 different positions of the oxygen vacancy in the crystal; the blue curve is the averaged spectrum.

at about 3.4 eV above the valence band edge, which coincides with the experimental peak position. This calculated peak intensity is proportional to the oxygen vacancies concentration, and the experimental peak is well described by the theoretical one obtained in the calculation of one vacancy per 96 atoms. Thus, the calculations confirm the conclusion that the Ar^+ ion bombardment generate the oxygen vacancies in the near-surface oxide layer and allows us to estimate the resulting vacancy concentration. The estimation of oxygen vacancy concentration in the studied films after the Ar^+ bombardment results in 8.7×10^{20} cm^{-3}. On the other hand, the calculated atomic ratio value [O]/[Zr+Hf] = 1.96 very well agrees to that obtained from the XPS analysis of the Hf4*f*, Zr3*d* and O1*s* levels. Note also that, after Ar^+ ion bombardment, a weak broadening of the upper edge of the studied oxides valence band is also observed. This feature is not explained by the presence of oxygen vacancies.

4. Conclusion

In the present study, the atomic and electronic structure of 25 nm thick $Hf_{0.5}Zr_{0.5}O_2$ and La-doped $Hf_{0.5}Zr_{0.5}O_2$ (with a La concentration of about 3.5%) films synthesized by ALD was investigated. According to the X-ray photoelectron spectroscopy, the La atoms in $Hf_{0.5}Zr_{0.5}O_2$:La are mainly in the form of La_2O_3. The bandgap value estimation from the energy loss spectrum of O1s photoelectrons for the $Hf_{0.5}Zr_{0.5}O_2$ and $Hf_{0.5}Zr_{0.5}O_2$:La results in a similar value of 5.4 eV. The bombardment of $Hf_{0.5}Zr_{0.5}O_2$ and $Hf_{0.5}Zr_{0.5}O_2$:La films with argon ions leads to the oxygen vacancies generation therein. The valence band photoelectron spectra of perfect $Hf_{0.5}Zr_{0.5}O_2$ and $Hf_{0.5}Zr_{0.5}O_2$:La orthorhombic crystals, calculated by the first principle simulation, very well describe the experimental spectra of the initial films, whereas the theoretical spectra for the crystals with oxygen vacancies (one vacancy per 96 atoms) explain the spectra of the films after their bombardment with argon ions for 5 minutes. The estimated oxygen vacancies concentration in the films after the Ar^+ bombardment is 8.7×10^{20} cm^{-3}. The calculated atomic ratio value [O]/[Zr+Hf] = 1.96 very well agrees with the value obtained from the analysis of the Hf4*f* and Zr3*d* core levels. For the initial samples, the sensitivity of X-ray photoelectron spectroscopy is not good enough to reveal the oxygen vacancies' concentration.

Declaration of competing interest

The authors declare that they have no known competing financial interests or personal relationships that could have appeared to influence the work reported in this paper.

Acknowledgments

This work was supported by the Russian Foundation for Basic Research, Grant №20-57-12003 (XPS measurements) and under the state contract with ISP SB RAS №0242-2021-0003 (DFT simulation), as well as by DFG Project No 430054035 (MI 1247/16-1).

References

[1] T. Schenk, M. Pesic, S. Slesazeck, U. Schroeder, T. Mikolajick, Memory technology-a primer for material scientists, Rep. Prog. Phys. 83 (2020) 086501.
[2] R. Materlik, C. Kunneth, M. Falkowski, T. Mikolajick, A. Kersch, Al-, Y-, and La-doping effects favoring intrinsic and field induced ferroelectricity in HfO_2: a first principles study, J. Appl. Phys. 123 (2018) 164101.
[3] S. Starschich, U. Boettger, An extensive study of the influence of dopants on the ferroelectric properties of HfO_2, J. Mater. Chem. C 5 (2017) 333–338.
[4] S. Mueller, J. Mueller, A. Singh, S. Riedel, J. Sundqvist, U. Schroeder, T. Mikolajick, Incipient ferroelectricity in Al-doped HfO_2 thin films, Adv. Funct. Mater. 22 (2012) 2412–2417.
[5] M.H. Park, Y.H. Lee, H.J. Kim, Y.J. Kim, T. Moon, K. Do Kim, J. Muller, A. Kersch, U. Schroeder, T. Mikolajick, C.S. Hwang, Ferroelectricity and antiferroelectricity of doped thin HfO_2-based films, Adv. Mater. 27 (2015) 1811–1831.
[6] M. Hoffmann, U. Schroeder, T. Schenk, T. Shimizu, H. Funakubo, O. Sakata, D. Pohl, M. Drescher, C. Adelmann, R. Materlik, A. Kersch, T. Mikolajick, Stabilizing the ferroelectric phase in doped hafnium oxide, J. Appl. Phys. 118 (2015), 072006.
[7] J. Robertson, R.M. Wallace, High-K materials and metal gates for CMOS applications, Mater. Sci. Eng. R Rep. 88 (2015) 1–41.
[8] V.A. Gritsenko, T.V. Perevalov, D.R. Islamov, Electronic properties of hafnium oxide: a contribution from defects and traps, Phys. Rep. 613 (2016) 1–20.
[9] D.R. Islamov, V.A. Gritsenko, T.V. Perevalov, V.S. Aliev, V.A. Nadolinny, A. Chin, Oxygen vacancies in zirconium oxide as the blue luminescence centres and traps responsible for charge transport: Part II – films, Materialia 15 (2021) 100980.
[10] D.R. Islamov, V.A. Gritsenko, T.V. Perevalov, V.A. Pustovarov, O.M. Orlov, A.G. Chernikova, A.M. Markeev, S. Slesazeck, U. Schroeder, T. Mikolajick, G.Y. Krasnikov, Identification of the nature of traps involved in the field cycling of $Hf_{0.5}Zr_{0.5}O_2$-based ferroelectric thin films, Acta Mater. 166 (2019) 47–55.
[11] D.R. Islamov, A.G. Chernikova, M.G. Kozodaev, A.M. Markeev, T.V. Perevalov, V.A. Gritsenko, O.M. Orlov, Charge transport mechanism in thin films of amorphous and ferroelectric $Hf_{0.5}Zr_{0.5}O_2$, JETP Lett. 102 (2015) 544–547.
[12] D.R. Islamov, T.V. Perevalov, Effect of oxygen vacancies on the ferroelectric $Hf_{0.5}Zr_{0.5}O_2$ stabilization: DFT simulation, Microelectron. Eng. 216 (2019) 111041.
[13] T. Mittmann, M. Materano, P.D. Lomenzo, M.H. Park, I. Stolichnov, M. Cavalieri, C.Z. Zhou, C.C. Chung, J.L. Jones, T. Szyjka, M. Muller, A. Kersch, T. Mikolajick, U. Schroeder, Origin of ferroelectric phase in undoped HfO2 films deposited by sputtering, Adv. Mater. Interfac. 6 (2019) 1900042.
[14] U. Schroeder, C. Richter, M.H. Park, T. Schenk, M. Pesic, M. Hoffmann, F.P.G. Fengler, D. Pohl, B. Rellinghaus, C.Z. Zhou, C.C. Chung, J.L. Jones, T. Mikolajick, Lanthanum-doped hafnium oxide: a robust ferroelectric material, Inorg. Chem. 57 (2018) 2752–2765.
[15] T. Szyjka, L. Baumgarten, T. Mittmann, Y. Matveyev, C. Schlueter, T. Mikolajick, U. Schroeder, M. Muller, Enhanced ferroelectric polarization in TiN/HfO2/TiN capacitors by interface design, ACS Appl. Electron. Ma 2 (2020) 3152–3159.
[16] W. Hamouda, C. Lubin, S. Ueda, Y. Yamashita, O. Renault, F. Mehmood, T. Mikolajick, U. Schroeder, R. Negrea, N. Barrett, Interface chemistry of pristine TiN/La: $Hf_{0.5}Zr_{0.5}O_2$ capacitors, Appl. Phys. Lett. 116 (2020) 252903.
[17] T.V. Perevalov, V.S. Aliev, V.A. Gritsenko, A.A. Saraev, V.V. Kaichev, Electronic structure of oxygen vacancies in hafnium oxide, Microelectron. Eng. 109 (2013) 21–23.
[18] T.V. Perevalov, A.K. Gutakovskii, V.N. Kruchinin, V.A. Gritsenko, I.P. Prosvirin, Atomic and electronic structure of ferroelectric La-doped HfO_2 films, Mater. Res. Express 6 (2019), 036403.
[19] T.V. Perevalov, V.A. Gritsenko, D.R. Islamov, I.P. Prosvirin, Electronic structure of oxygen vacancies in the orthorhombic noncentrosymmetric phase $Hf_{0.5}Zr_{0.5}O_2$, JETP Lett. 107 (2018) 55–60.
[20] P. Giannozzi, O. Andreussi, T. Brumme, O. Bunau, M.B. Nardelli, M. Calandra, R. Car, C. Cavazzoni, D. Ceresoli, M. Cococcioni, N. Colonna, I. Carnimeo, A. Dal Corso, S. de Gironcoli, P. Delugas, R.A. DiStasio, A. Ferretti, A. Floris, G. Fratesi, G. Fugallo, R. Gebauer, U. Gerstmann, F. Giustino, T. Gorni, J. Jia, M. Kawamura, H.Y. Ko, A. Kokalj, E. Kucukbenli, M. Lazzeri, M. Marsili, N. Marzari, F. Mauri, N.L. Nguyen, H.V. Nguyen, A. Otero-de-la-Roza, L. Paulatto, S. Ponce, D. Rocca, R. Sabatini, B. Santra, M. Schlipf, A.P. Seitsonen, A. Smogunov, I. Timrov, T. Thonhauser, P. Umari, N. Vast, X. Wu, S. Baroni, Advanced capabilities for materials modelling with QUANTUM ESPRESSO, J. Phys-Condens. Mat. 29 (2017) 465901.
[21] M. Lederer, T. Kampfe, R. Olivo, D. Lehninger, C. Mart, S. Kirbach, T. Ali, P. Polakowski, L. Roy, K. Seidel, Local crystallographic phase detection and texture mapping in ferroelectric Zr doped HfO_2 films by transmission-EBSD, Appl. Phys. Lett. 115 (2019) 222902.
[22] L. Sha, R. Puthenkovilakam, Y.S. Lin, J.P. Chang, Ion-enhanced chemical etching of HfO_2 for integration in metal-oxide-semiconductor field effect transistors, J. Vac. Sci. Technol. B 21 (2003) 2420–2427.
[23] R. Jiang, E.Q. Xie, Z.F. Wang, Interfacial chemical structure of HfO_2/Si film fabricated by sputtering, Appl. Phys. Lett. 89 (2006) 142907–142910.
[24] M.S. Kim, Y.D. Ko, J.H. Hong, M.C. Jeong, J.M. Myoung, I. Yun, Characteristics and processing effects of ZrO_2 thin films grown by metal-organic molecular beam epitaxy, Appl. Surf. Sci. 227 (2004) 387–398.
[25] S. Tsunekawa, K. Asami, S. Ito, M. Yashima, T. Sugimoto, XPS study of the phase transition in pure zirconium oxide nanocrystallites, Appl. Surf. Sci. 252 (2005) 1651–1656.
[26] A. Sharma, M. Varshney, S. Kang, J. Baik, T.-K. Ha, K.-H. Chae, S. Kumar, H.-J. Shin, Electronic structure study and dielectric properties of amorphous ZrO_2 and HfO_2, Adv. Mater. Lett. 7 (2016) 17–22.
[27] I. Bespalov, M. Datler, S. Buhr, W. Drachsel, G. Rupprechter, Y. Suchorski, Initial stages of oxide formation on the Zr surface at low oxygen pressure: an *in situ* FIM and XPS study, Ultramicroscopy 159 (2015) 147–151.

[28] F. Ambriz-Vargas, G. Kolhatkar, R. Thomas, R. Nouar, A. Sarkissian, C. Gomez-Yanez, M.A. Gauthier, A. Ruediger, Tunneling electroresistance effect in a Pt/Hf0.5Zr0.5O2/Pt structure, Appl. Phys. Lett. 110 (2017), 093106.
[29] T.V. Perevalov, D.R. Islamov, V.A. Gritsenko, I.P. Prosvirin, Electronic structure of stoichiometric and oxygen-deficient ferroelectric Hf0.5Zr0.5O2, Nanotechnology 29 (2018) 194001.
[30] C.V. Ramana, R.S. Vemuri, V.V. Kaichev, V.A. Kochubey, A.A. Saraev, V.V. Atuchin, X-ray photoelectron spectroscopy depth profiling of La_2O_3/Si thin films deposited by reactive magnetron sputtering, ACS Appl. Mater. Inter. 3 (2011) 4370–4373.
[31] M.F. Sunding, K. Hadidi, S. Diplas, O.M. Lovvik, T.E. Norby, A.E. Gunnaes, XPS characterisation of in situ treated lanthanum oxide and hydroxide using tailored charge referencing and peak fitting procedures, J. Electron. Spectrosc. Relat. Phenom. 184 (2011) 399–409.
[32] X.B. Lou, X. Gong, J. Feng, R. Gordon, Band-offset analysis of atomic layer deposition La_2O_3 on GaAs(111), (110), and (100) surfaces for epitaxial growth, ACS Appl. Mater. Inter. 11 (2019) 28515–28519.
[33] P. Burroughs, A. Hamnett, A.F. Orchard, G. Thornton, Satellite structure in X-ray photoelectron-spectra of some binary and mixed oxides of lanthanum and cerium, J. Chem. Soc. Dalton (1976) 1686–1698.
[34] J.P.H. Li, X.H. Zhou, Y.Q. Pang, L. Zhu, E.I. Vovk, L.N. Cong, A.P. van Bavel, S.G. Li, Y. Yang, Understanding of binding energy calibration in XPS of lanthanum oxide by in situ treatment, Phys. Chem. Chem. Phys. 21 (2019) 22351–22358.